

UDC 621.763 + 621.762.24

<https://doi.org/10.17073/0021-3438-2024-2-44-54>

Research article

Научная статья



## Synthesis and study of the properties of zirconium dioxide powders with different yttrium content

S.V. Buinachev<sup>1,2</sup>, M.A. Domashenkov<sup>1,2</sup>, M.A. Mashkovtsev<sup>2</sup>, D.O. Polivoda<sup>2</sup>, N.V. Zhirenkina<sup>1</sup>

<sup>1</sup> Ural Federal University named after the first President of Russia B.N. Yeltsin  
19 Mira Str., Yekaterinburg, Sverdlovsk region 620002, Russia

<sup>2</sup> Institute of High-Temperature Electrochemistry of the Ural Branch of the Russian Academy of Sciences  
20 Akademicheskaya Str., Yekaterinburg 620066, Russia

✉ Maksim A. Domashenkov (maks84155@gmail.com)

**Abstract:** As part of the study, the influence of yttrium content on the properties of particles during controlled precipitation and after thermal treatment was investigated. Precipitation was carried out at a constant pH of 5 from nitric acid solutions, where the concentration of zirconium was 1 mole/dm<sup>3</sup> and the yttrium content ranged from 0 to 30 % based on their oxides. The drying and calcination temperatures of the precipitates were 40 °C and 1000 °C, respectively. It was shown that with a yttrium content of up to 15 %, there was a consistent increase in the average diameter of zirconium hydroxide particles during deposition. When the yttrium concentration was increased to 30 %, the average particle size increased during the first 10 minutes of deposition, followed by a gradual decrease. The largest particle diameter was observed in the specimen with 7 % yttrium. In all cases, the formation of spherical aggregates was observed. With an increasing yttrium content, the boundaries between particles became smoother, and the degree of co-deposition of yttrium during synthesis decreased from 80 % to 60 %. Depending on the yttrium concentration, different modifications of stabilized zirconium dioxide powders were obtained: tetragonal ZrO<sub>2</sub> for 2–7 % yttrium, and cubic ZrO<sub>2</sub> for 15–30 % yttrium. Therefore, the results obtained during the study can be useful for the development of technology for the production of powdered materials for various applications.

**Key words:** stabilized zirconium dioxide, deposition, aggregation, thermal barrier coatings.

**For citation:** Buinachev S.V., Domashenkov M.A., Mashkovtsev M.A., Polivoda D.O., Zhirenkina N.V. Synthesis and study of the properties of zirconium dioxide powders with different yttrium content. *Izvestiya. Non-Ferrous Metallurgy*. 2024;30(2):44–54.

<https://doi.org/10.17073/0021-3438-2024-2-44-54>

## Синтез и исследование свойств порошков диоксида циркония с различным содержанием иттрия

С.В. Буйначев<sup>1,2</sup>, М.А. Домашенков<sup>1,2</sup>, М.А. Машковцев<sup>2</sup>, Д.О. Поливода<sup>2</sup>, Н.В. Жиренкина<sup>1</sup>

<sup>1</sup> Уральский федеральный университет имени первого Президента России Б.Н. Ельцина  
Россия, 620002, Свердловская обл., г. Екатеринбург, ул. Мира, 19

<sup>2</sup> Институт высокотемпературной электрохимии УрО РАН  
Россия, 620066, Свердловская обл., г. Екатеринбург, ул. Академическая, 20

✉ Максим Александрович Домашенков (maks84155@gmail.com)

**Аннотация:** В рамках работы проведено изучение влияния содержания иттрия на изменение свойств частиц как в ходе контролируемого осаждения, так и после термообработки. Осаждение проводили при постоянном значении pH = 5 из азотно-кис-

лых растворов, где концентрация циркония составляла 1 моль/дм<sup>3</sup>, а содержание иттрия – от 0 до 30 % в пересчете на их оксиды. Температуры сушки и обжига осадков составляли 40 и 1000 °С соответственно. Показано, что при содержании Y вплоть до 15 % происходит постоянное увеличение среднего диаметра частиц гидроксида циркония в процессе осаждения, при повышении концентрации Y до 30 % средний размер частиц возрастает в течение первых 10 мин осаждения, после чего происходит его плавное снижение. Наибольший диаметр частиц наблюдался у образца с 7 % Y. Во всех случаях отмечено формирование сферидальных агрегатов. При этом с повышением содержания Y происходят сглаживание границ между частицами и снижение степени соосаждения Y в процессе синтеза с 80 до 60 %. В зависимости от концентрации иттрия получены различные модификации порошков стабилизированного диоксида циркония: при 2–7 % Y – тетрагональный ZrO<sub>2</sub>, а при 15–30 % Y – кубический ZrO<sub>2</sub>. Таким образом, полученные в ходе исследований результаты могут быть полезны для разработки технологии производства порошковых материалов для различного применения.

**Ключевые слова:** стабилизированный диоксид циркония, осаждение, агрегация, термобарьерные покрытия.

**Для цитирования:** Буйначев С.В., Домашенков М.А., Машковцев М.А., Поливода Д.О., Жиренкина Н.В. Синтез и исследование свойств порошков диоксида циркония с различным содержанием иттрия. *Известия вузов. Цветная металлургия*. 2024;30(2):44–54. <https://doi.org/10.17073/0021-3438-2024-2-44-54>

## Introduction

Stabilized zirconium dioxide is used in many industrial fields, including the creation of thermal barrier coatings [1–3], the manufacturing of ceramic products for medical applications [4–6], and the production of solid oxide electrolytes for electrochemical devices [7–9]. It has low thermal conductivity [10], high chemical and corrosion resistance [11], good oxygen conductivity, and biological compatibility with human tissues [12].

To generate thermal barrier coatings on gas turbine engine components, the atmospheric plasma spraying (APS) method is often used, utilizing yttria-stabilized zirconia (YSZ) powders [13–15]. YSZ powder should have high bulk density, low specific surface area, spheroidal particle shape ranging from 20 to 100 μm, and high flowability [16]. Coatings obtained using APS technology reduce part erosion rates and increase adhesion and corrosion resistance during thermal cycling at high temperatures [17].

YSZ powders are also used in the production of ingots for vacuum electron beam evaporation [18]. These ingots are used to form columnar-structured thermal barrier coatings on gas turbine engine blades [19–21]. Compared to APS coatings, columnar coatings have higher adhesion resistance, lower elastic modulus, and surface roughness [22].

Common methods for obtaining stabilized zirconium dioxide in industry include direct and reverse precipitation of zirconium hydroxides [23], the sol-gel process [24], and spray pyrolysis [25]. However, all these methods do not allow for the control of the properties of precipitates and, therefore, the final powder materials. It is known that when using precipitation methods, the properties of hydroxide precipitates strongly depend on pH [26].

Direct and reverse precipitation usually result in fragmented particle shapes and wide size distribution. The sol-gel method is often used to synthesize fine-dispersed powders using organic binders and solvents, which complicates the technology and scaling process. Spray pyrolysis can produce particles with a spheroidal shape ranging from several nanometers to several micrometers. However, obtaining coarse particles with a diameter of 20 to 100 μm is practically impossible. The method is quite complex in technical implementation, requiring high temperatures and posing scaling challenges.

Authors [27] have shown that by varying the pH value during controlled precipitation, it is possible to obtain zirconium hydroxide with different properties, such as average particle diameter and shape, specific surface area, and porosity. It has also been found that the addition of yttrium during this process leads to further modification of these properties.

Thus, precipitation under controlled conditions can be a promising method for synthesizing hydroxide materials with required properties for use in various industrial fields.

In this study, the influence of yttrium content during controlled precipitation at a constant pH of 5 on the properties of zirconium and yttrium hydroxide precipitates, as well as the resulting powders after thermal treatment, was investigated. Specimens of zirconium oxide with yttrium content up to 30 % were obtained. An analysis of particle size distribution and shape was performed during precipitation and after annealing. The degree of yttrium co-precipitation and the phase composition of the powders after annealing were also studied.

## Materials and methods

The synthesis of zirconium hydroxide with varying yttrium content was carried out by the controlled precipitation method at a constant pH of 5. The initial solutions of zirconium and yttrium nitrates were prepared by dissolving zirconium carbonate and yttrium oxide in nitric acid. A 10 % ammonia solution was used as the precipitant. Before each precipitation, a solution containing 123 g of zirconium in terms of oxide and the calculated amount of yttrium to achieve concentrations of 0, 2, 4, 7, 15, and 30 % in terms of oxide in the final powder (referred to as specimens 0%Y, 2%Y, 4%Y, 7%Y, 15%Y, and 30%Y, respectively) was prepared.

The precipitation was carried out in a 3-liter glass beaker with constant stirring using an overhead stirrer. The combined solution of zirconium and yttrium nitrates was dosed into the reactor using a peristaltic pump at a rate of 5 mL/min. The precipitant solution was introduced using another peristaltic pump, which was connected to a pH meter through a relay control system to control the dosing of ammonia and maintain constant pH. The precipitation process was carried out for 200 minutes, after which yttrium was further precipitated by raising the pH to 8 for specimens with yttrium addition. The suspension was then filtered using a vacuum Buchner filter, dried at 40 °C for 24 h, and fired at 1000 °C.

The average particle diameter and their size distribution were determined using laser diffraction on an Analysette 22 instrument (“Fritch”, Germany) in the measurement range of 0.08 to 2000  $\mu\text{m}$  using green and infrared lasers. Suspension specimens were taken from the reactor at different stages during the precipitation for this purpose. The particle shape was evaluated using an optical microscope GX71 (“OLYMPUS”, Japan). The yttrium concentration in the mother solution was determined by complexometric titration using Trilon B. X-ray diffraction patterns of the specimens were obtained using an X’Pert Pro MPD diffractometer (“PANalytical B.V.”, Netherlands) with a solid-state pixel detector in  $\text{CuK}\alpha$  radiation with a  $\beta$ -filter. The phase composition and lattice parameters were determined by full-profile Rietveld analysis, and the areas of coherent scattering (ACS) were determined using the Scherrer method based on the most intense reflections at small scattering angles (shape factor  $K = 0.9$ ) using the X’Pert High Score Plus software (Netherlands).

## Results and discussion

Figure 1 shows the change in average particle diameter ( $d$ ) and size dispersion as a function of precipita-

tion duration ( $\tau$ ). It is shown that in the 0%Y specimen, the value of  $d$  increased starting from the 5<sup>th</sup> minute of the precipitation process and reached 33  $\mu\text{m}$  by the 200<sup>th</sup> minute. The addition of 2 % and 4 % yttrium led to a significant increase in this parameter throughout the precipitation process, reaching 38  $\mu\text{m}$  by the 200<sup>th</sup> minute. In the 7%Y specimen, an even greater increase in particle size was observed, reaching 40  $\mu\text{m}$  by the end of the deposition. Adding 15% Y resulted in a substantial increase in the average particle diameter to 39  $\mu\text{m}$  during the first 100 minutes of deposition, after which it remained almost unchanged. For the 30%Y specimen, a sharp increase in the value of  $d$  was recorded by the 20<sup>th</sup> minute of deposition, reaching 28  $\mu\text{m}$ , after which it gradually decreased to 23  $\mu\text{m}$  by the completion of the process.

The size dispersion parameter for the 0%Y specimen decreased throughout the precipitation process, reaching 1.08 by the 200<sup>th</sup> minute. For specimens with yttrium content ranging from 2 % to 15 %, the values of this parameter decreased by the 70<sup>th</sup> minute of deposition, after which they started to increase, ending the process in the range of 1.2 to 1.28. For the 30%Y specimen, the size dispersion value was consistently higher throughout the precipitation compared to the other specimens, reaching 1.3 by the 200<sup>th</sup> minute.

Figure 2 illustrates the mass size distribution of particles as a function of precipitation time and yttrium addition. For specimens with yttrium content ranging from 0 to 15 %, a peak in the range of  $\tau = 15\div 20 \mu\text{m}$  with an arm in the range of  $d = 1\div 5 \mu\text{m}$  formed during the first 10 minutes of deposition. As the precipitation time increases, this peak disappears, and a peak at  $d \sim 1 \mu\text{m}$  with a mass fraction of less than 1 % emerges. Simultaneously, the main peak shifts uniformly towards larger sizes, indicating an increase in the average particle diameter. The peak at  $d \sim 1 \mu\text{m}$  remains relatively unchanged in its position. For the 30%Y specimen, a peak in the range of  $d \sim 30 \mu\text{m}$  with an arm in the range of  $d = 1\div 5 \mu\text{m}$  is formed by the 10<sup>th</sup> minute of deposition. With increasing precipitation time, the main peak shifts towards smaller sizes, and the arm transforms into a separate peak with a maximum in the range of  $d = 1\div 2 \mu\text{m}$ .

It is likely that the formation of two populations of particles during precipitation leads to an increase in their average diameter due to layer-by-layer aggregation. Apparently, conducting hydrolysis at constant pH results in the formation of similarly charged primary nuclei, which aggregate upon collision to form larger particles,

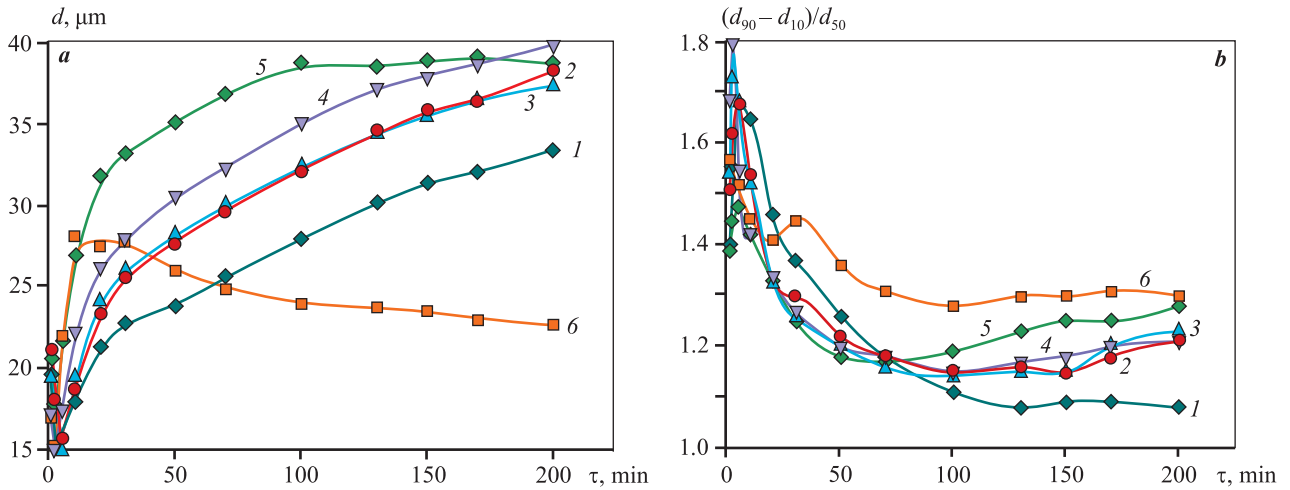


**Fig. 1.** Average particle size (a) and dispersion of sizes (b) as a function of precipitation duration

1 – sample 0%Y; 2 – 2%Y; 3 – 4%Y; 4 – 7%Y; 5 – 15%Y; 6 – 30%Y

**Рис. 1.** Изменение среднего диаметра частиц (a) и дисперсии размеров (b) в зависимости от длительности осаждения

1 – образец 0%Y; 2 – 2%Y; 3 – 4%Y; 4 – 7%Y; 5 – 15%Y; 6 – 30%Y

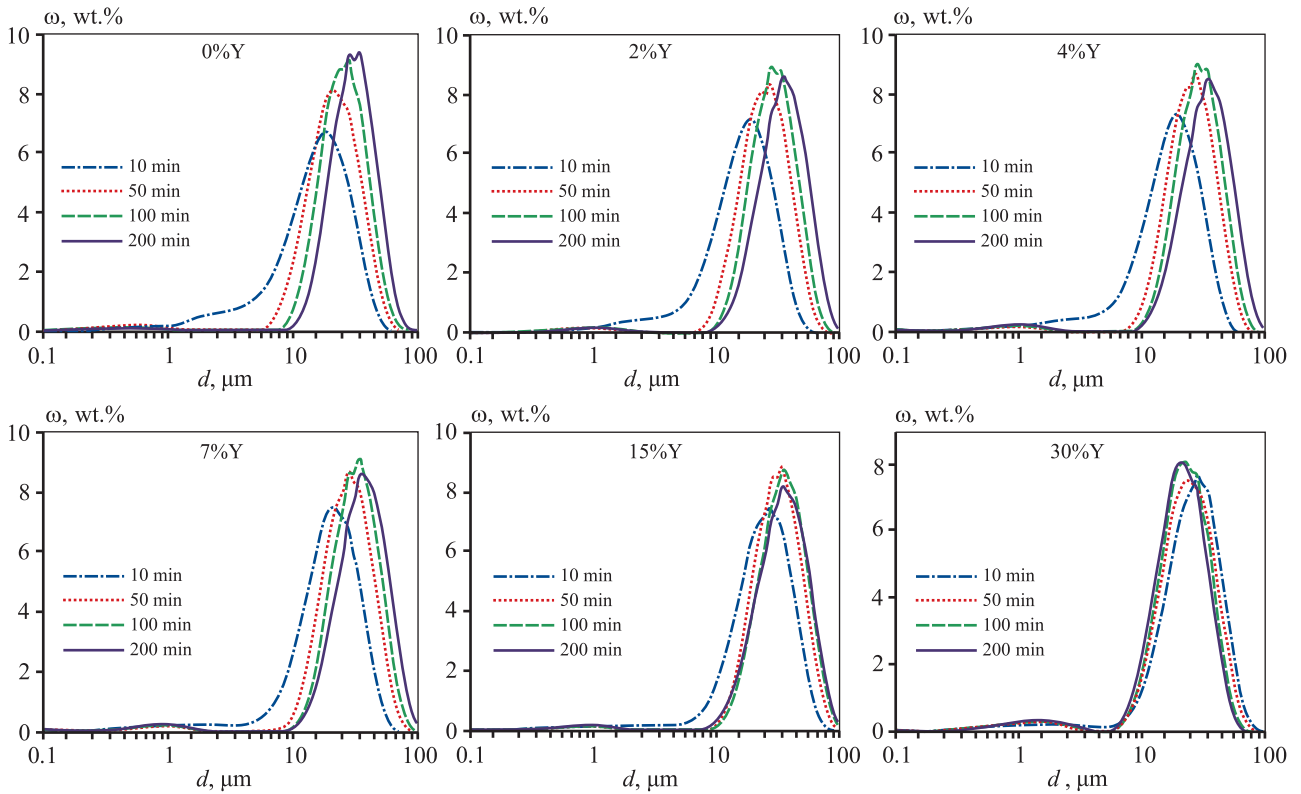


**Fig. 2.** Mass distribution of particle sizes as a function of precipitation duration

**Рис. 2.** Массовое распределение частиц по размерам в зависимости от длительности осаждения исследуемых образцов

followed by a change in charge on the surface due to olation processes.

Thus, the simultaneous occurrence of nucleation with one charge and the appearance of larger particles

with the opposite charge serve as the basis for the mechanism of aggregation processes. The addition of yttrium during precipitation appears to significantly affect the progress of olation and oxolation processes. It can

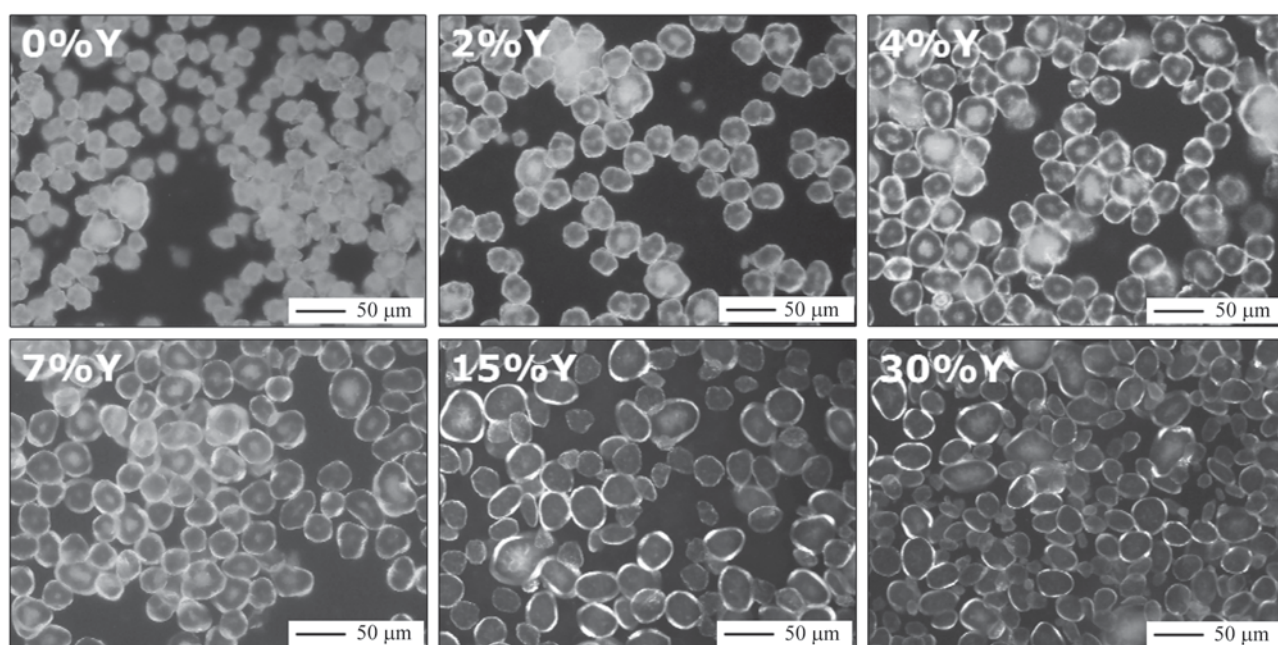
be assumed that its presence leads to an increase in the surface charge of primary particles, which hinders their aggregation with each other. These nuclei predominantly begin to accumulate on the formed large aggregates with the opposite charge, resulting in a significant increase in the average particle diameter when yttrium is added. However, at a yttrium content of 30 %, the layer-by-layer aggregation process is hindered, and the large aggregates stop increasing in size, leading to an increase in the fraction of small particles. Presumably, the high yttrium content almost completely suppresses the flocculation processes and neutralizes the charge on the surface of large aggregates, resulting in an increase in the size of particles in those aggregates where the charge has not yet been neutralized.

Figure 3 illustrates optical images of particles at the 200<sup>th</sup> minute of sedimentation for specimens with different yttrium content. It is shown that in the specimen without the addition of Y, the formation of spheroidal aggregates with well-defined but rough boundaries occurs. A gradual increase in yttrium content leads to the formation of spheroidal aggregates with smoother boundaries. It has been found that the introduction of yttrium up to 15 % results in an increase in particle and aggregate sizes, while increasing its content to 30 % leads to a decrease, which is consistent with laser diffraction results.

The influence of yttrium addition on the shape of particles can be explained by the same approach used in the analysis of particle size changes, based on the difference in their charges. As mentioned earlier, the addition of yttrium hinders aggregation of primary particles, leading primarily to increased collisions between very small primary particles and larger ones, thereby contributing to the formation of smooth boundaries on the surface.

Figure 4 shows the change in the concentration of yttrium cations ( $Y^{3+}$ ) in the suspension during precipitation and the rate of co-precipitation of yttrium with zirconium hydroxide as a function of process time. It is shown that for specimens with 2%Y, 4%Y, 7%Y, and 15%Y, there is a gradual increase in  $Y^{3+}$  concentration with increasing sedimentation time, reaching 0.3, 3.0, 5.5, and 15 g/dm<sup>3</sup>, respectively, by the end of the process. For the 30%Y specimen, there is a sharp increase in  $Y^{3+}$  content to 60 g/dm<sup>3</sup> by the 100<sup>th</sup> minute of the process, after which it remains nearly constant. At the same time, the rate of yttrium co-precipitation with zirconium hydroxide reaches 80 % by the 200<sup>th</sup> minute for the 2%Y, 4%Y, and 7%Y specimens, and 72 % and 60 % for the 15%Y and 30%Y specimens, respectively.

Thus, despite the low pH value of the sedimentation process, a significant portion of yttrium is captured by the zirconium hydroxide precipitate. This is likely due to



**Fig. 3.** Optical images of particles of the investigated specimens by the 200<sup>th</sup> minute of deposition

**Рис. 3.** Оптические изображения частиц исследуемых образцов к 200-й минуте осаждения

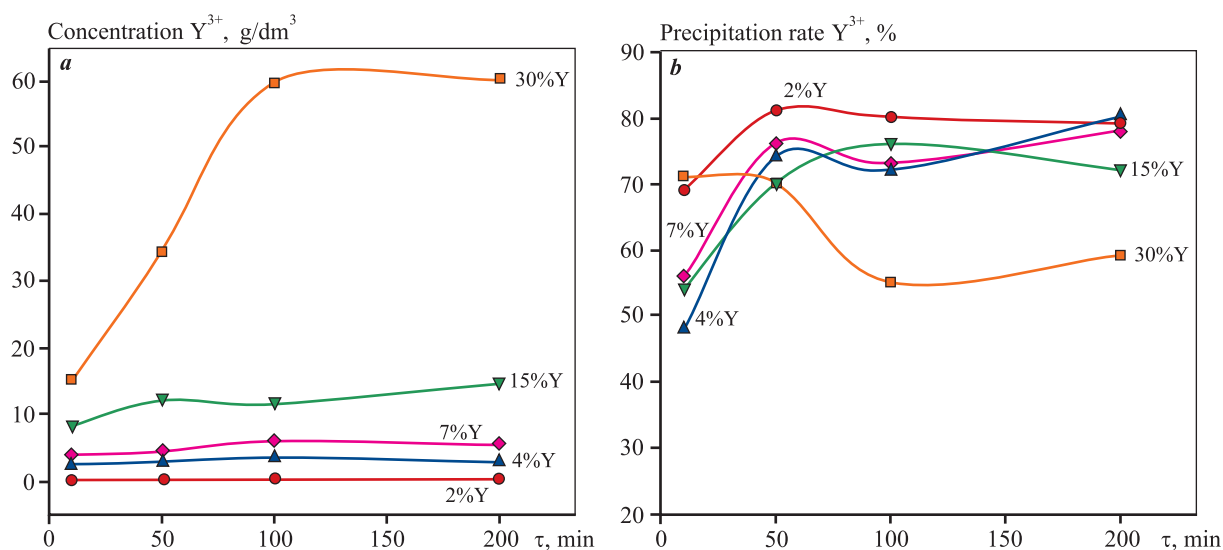


**Fig. 4.** Concentration (a) and co-deposition rate (b) of yttrium cations in slurry as a function of precipitation duration

**Рис. 4.** Изменение концентрации (a) и степени соосаждения (b) катионов иттрия в суспензии в зависимости от длительности осаждения

the high (excessive) concentration of  $OH^-$  groups on the surface of the hydroxide, which bind to the  $Zr^{4+}$  cations during the formation of zirconium hydroxide.

Figure 5 shows the change in the average particle diameter and size dispersion as a function of the synthesis stage for the specimens. It is shown that the values of  $d$  decrease stepwise after drying at  $t = 40^\circ C$  and annealing at  $1000^\circ C$ . After annealing, the average particle size for the 0%Y specimen was  $22\ \mu m$ , for the 2%Y–15%Y specimens it remained at around  $25\ \mu m$ , and for the 30%Y specimen it was  $17\ \mu m$ . The size dispersion values after annealing for specimens with yttrium content up to 15 % are practically at the same level, around 1.1, and for the 30%Y specimen they are around 1.4.

Figure 6 illustrates the particle size distribution as a function of the stage of specimen synthesis. For specimens with yttrium content up to 15 %, after annealing at  $1000^\circ C$ , a narrow, high peak is observed, which, compared to the suspension and drying stages, has significantly shifted to the left, indicating smaller particle sizes. At the same time, the shape of the peak has not changed significantly, suggesting that neither destruction nor additional aggregation occurs during heat treatment. For the specimen with 30 % yttrium, the particle size distribution after annealing looks similar, but the distribution peak is wider and lower compared to the other specimens. This may be due to the fact that even at the precipitation stage, large aggregates hardly changed in size, while a large number of new aggregates were formed.

Figure 7 shows optical images of particles after annealing at  $1000^\circ C$  for specimens with different yttrium contents. It is shown that for all of them, after annealing, the particles retain a spheroidal shape. Specimens with 0%Y, 2%Y, and 4%Y exhibit particles with uneven boundaries, while specimens with 7%Y, 15%Y, and 30%Y display particles with smoother boundaries.

It is known that zirconium dioxide can exist in three different crystalline modifications depending on temperature: monoclinic at room temperature, tetragonal at  $t > 1170^\circ C$ , and cubic at  $t > 2370^\circ C$ . To increase its thermal stability, stabilizing components are introduced, with yttrium oxide being the most common. The similarity of the ionic radii of Zr and Y, as well as the isomorphism of their structures, allows for the formation of a solid solution when Y is introduced into the crystal lattice of  $ZrO_2$ . Stabilization of zirconium dioxide with low-valent cations can lead to the stabilization of the tetragonal or cubic phase at lower temperatures, even at room temperature. This is due to the generation of oxygen vacancies in the lattice, which in turn reduces the stress caused by the energetically unfavorable 8-coordinated configuration [28].

Depending on the yttrium content, three structural modifications of zirconia oxide were obtained after annealing at  $1000^\circ C$ . The data from X-ray phase analysis are presented in Table 1. Zirconium oxide without yttrium addition has a monoclinic structural modification, with a crystallite size of  $48\ nm$ . Specimens with 2 %,

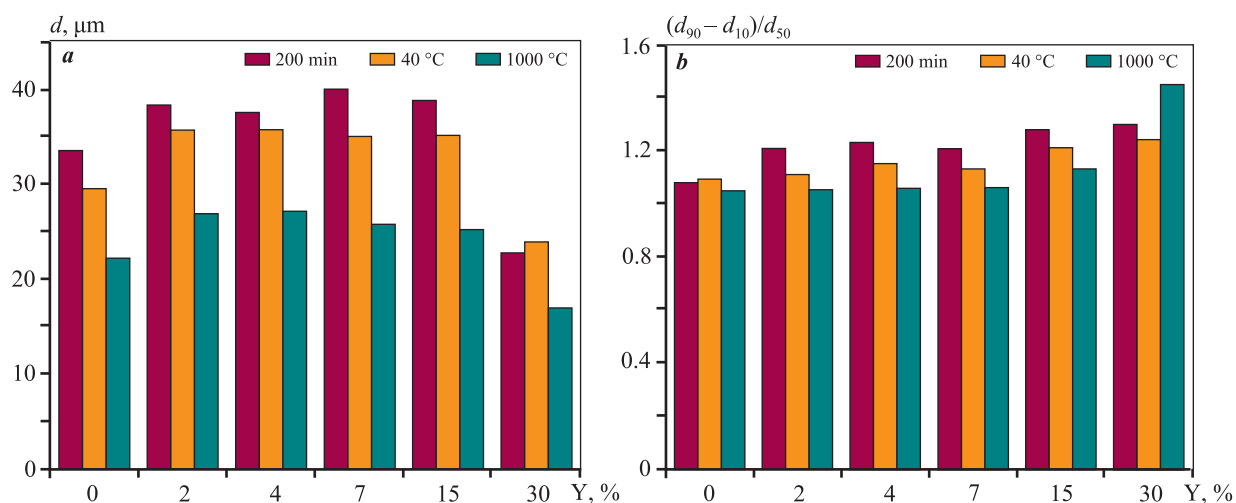


Fig. 5. Average particle size (a) and dispersion of sizes (b) at various stages of synthesis of the considered specimens

Рис. 5. Значения среднего диаметра частиц (a) и дисперсии размеров (b) на разных этапах синтеза исследуемых образцов

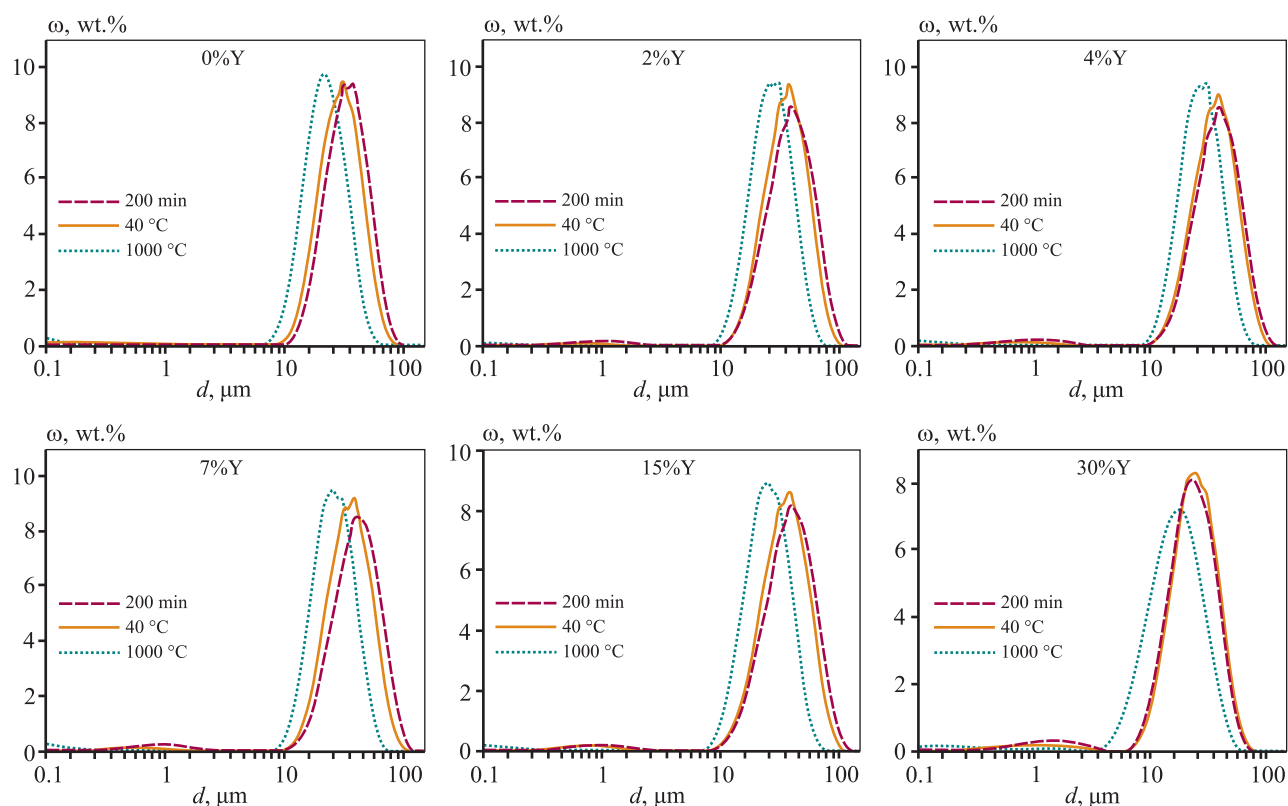


Fig. 6. Particle size distribution at various stages of synthesis of the considered specimens

Рис. 6. Распределение частиц по размерам на разных этапах синтеза исследуемых образцов

4 %, and 7 % Y content are characterized by a tetragonal modification. This is confirmed by the smaller values of edge lengths compared to the monoclinic modification. The crystallite size decreases with increasing yttrium content, which is consistent with literature data [29], and ranges from 40 to 60 nm. At the same

time, zirconium dioxide with 15 % and 30 % Y additions undergoes the formation of a cubic modification, as evidenced by the similar edge length parameters. The crystallite sizes are 28 and 42 nm, respectively. The X-ray diffraction patterns of all yttrium-modified specimens do not show peaks corresponding to pure

**X-ray phase analysis of zirconium dioxide with various content of yttrium**

Результаты рентгенофазового анализа образцов диоксида циркония с различным содержанием иттрия

Specimen	Crystallite size, nm	Modification type	Lattice constants, Å		
			<i>a</i>	<i>b</i>	<i>c</i>
0%Y	48	Monoclinic	5.147	5.202	5.312
2%Y	60	Tetragonal	3.595	3.595	5.175
4%Y	51	Tetragonal	3.603	3.603	5.170
7%Y	42	Tetragonal	3.614	3.614	5.153
15%Y	28	Cubic	5.127	5.127	5.127
30%Y	42	Cubic	5.142	5.142	5.142

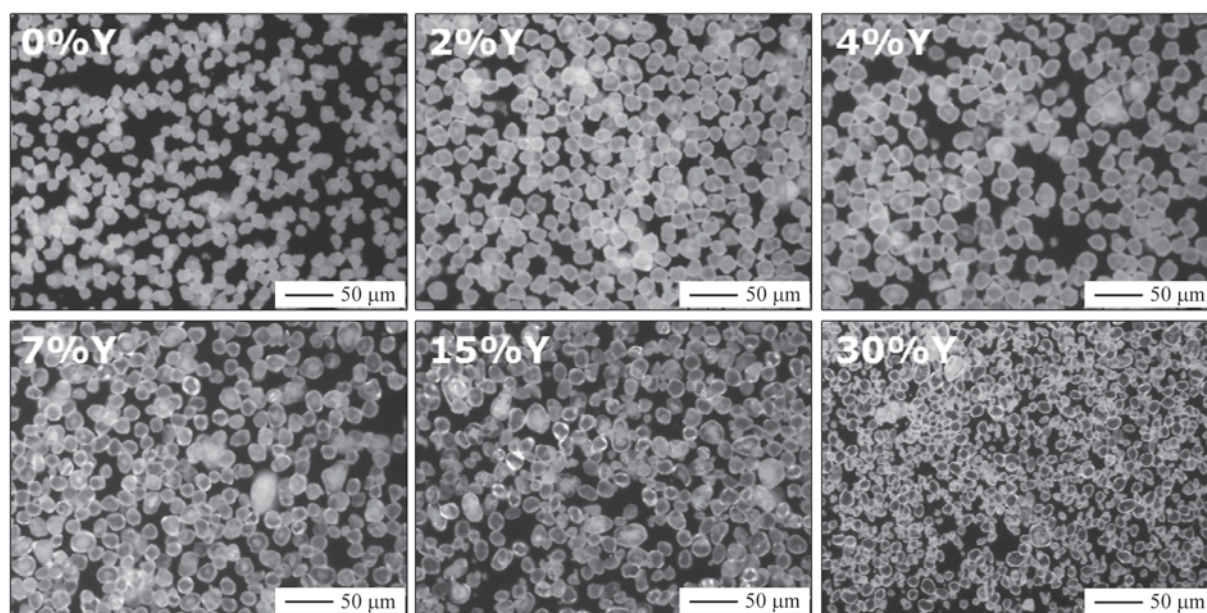


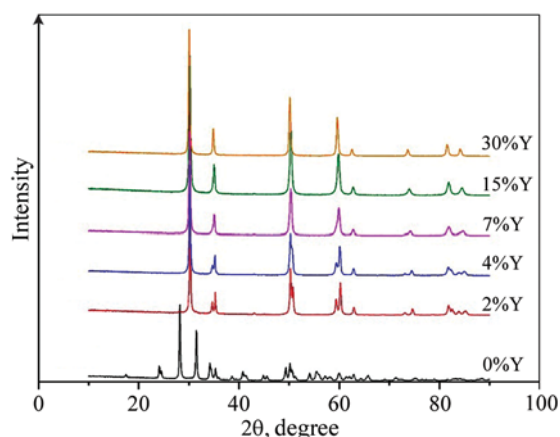
Fig. 7. Optical images of particles after annealing at 1000 °C

Рис. 7. Оптические изображения частиц после обжига при 1000 °C исследуемых образцов

yttrium oxide, indicating that it is uniformly distributed in zirconium dioxide, forming a solid substitution solution.

**Conclusions**

The specimens of zirconium dioxide with varying yttrium content were produced in this study through controlled precipitation at constant pH. The influence of yttrium addition on the average particle diameter, size dispersion, particle size distribution, shape, degree of yttrium deposition, and phase composition of the final powders was investigated. A mechanism for the aggregation of zirconium hydroxide during precipitation at a constant pH value was proposed, and the influence of yttrium addition on this process was examined.

Fig. 8. X-ray patterns of the considered specimens after annealing at  $t = 1000$  °CРис. 8. Рентгенограммы исследуемых образцов после обжига при  $t = 1000$  °C

It was found that the yttrium content significantly influenced the particle size during deposition: in specimens without yttrium, the average particle diameter was 33  $\mu\text{m}$ , while with 7 % yttrium addition, it increased to 40  $\mu\text{m}$ . It was also observed that yttrium co-deposited with zirconium hydroxide at a pH of 5 during the precipitation process, with the degree of yttrium precipitation ranging from 60 % to 80 % depending on its content.

After thermal treatment, there was no destruction or additional aggregation of particles, and the spherical shape of the particles was preserved, with low size dispersion observed in all specimens. Different modifications of zirconium dioxide were obtained depending on the yttrium content: monoclinic for specimens without yttrium, tetragonal for 2–7 % yttrium addition, and cubic for over 15 % yttrium addition.

Therefore, the obtained results can be useful in the development of powder production technology for various industrial applications, particularly for the formation of thermal barrier coatings using atmospheric plasma spraying.

## References

1. Qiaomu L., Shunzhou H., Aijie H. Composite ceramics thermal barrier coatings of yttria stabilized zirconia for aero-engines. *Journal of Materials Science & Technology*. 2019;35(12):2814–2823. <https://doi.org/10.1016/j.jmst.2019.08.003>
2. Liu G., Shen Z., He L., Mu R., Huang G. LaYZrO/YSZ double ceramic layer thermal barrier coatings by EB-PVD: Thermal performance, morphology and failure behavior. *Materialia*. 2023;27:101661. <https://doi.org/10.1016/j.mtla.2022.101661>
3. Erdoğlan N.N., Başıyğit A.B. Investigating thermal shock and corrosion resistance of Inconel 601 super alloy after thermal barrier coating with 8 % YSZ powder. *Materials Today Communications*. 2023;36:106516. <https://doi.org/10.1016/j.mtcomm.2023.106516>
4. Moayedee Y., Nikzad L., Habibzadeh S. Mechanical, electrochemical, and biological properties of YSZ-Mo: A new class of bio-composites. *Materialia*. 2022;24:101515. <https://doi.org/10.1016/j.mtla.2022.101515>
5. Piconi C., Maccauro G. Zirconia as a ceramic biomaterial. *Biomaterials*. 1999;20(1):1–25. [https://doi.org/10.1016/S0142-9612\(98\)00010-6](https://doi.org/10.1016/S0142-9612(98)00010-6)
6. Xiuping Z., Xin W., Jing S. Additive manufacturing of zirconia ceramics: a state-of-the-art review. *Journal of Materials Research and Technology*. 2020;9(4):9029–9048. <https://doi.org/10.1016/j.jmrt.2020.05.131>
7. Xiuan X., Hiroya A., Kazuo K., Ryo H., Anze S., Makio N. Novel Co-precipitation method to synthesize NiO–YSZ nanocomposite powder for solid oxide fuel cell. *Advanced Powder Technology*. 2014;25(2):490–494. <https://doi.org/10.1016/j.apt.2013.08.001>
8. Shao Z., Zhou W., Zhu Z. Advanced synthesis of materials for intermediate-temperature solid oxide fuel cells. *Progress in Materials Science*. 2012;57(4):804–874. <https://doi.org/10.1016/j.pmatsci.2011.08.002>
9. Monaco F., Effori E., Hubert M., Siebert E., Geneste G., Morel B., Djurado E., Montinaro D., Laurencin J. Electrode kinetics of porous Ni–3YSZ cermet operated in fuel cell and electrolysis modes for solid oxide cell application. *Electrochimica Acta*. 2021;389(1):138765. <https://doi.org/10.1016/j.electacta.2021.138765>
10. Jungwan C., Joonsuk P., Jihwan A. Low thermal conductivity of atomic layer deposition yttria-stabilized zirconia (YSZ) thin films for thermal insulation applications. *Journal of the European Ceramic Society*. 2017;37(9):3131–3136. <https://doi.org/10.1016/j.jeurceramsoc.2017.03.045>
11. Raheleh A.-P., Reza S.-R., Reza M., Hossein J. Improving the hot corrosion resistance of plasma sprayed ceria–yttria stabilized zirconia thermal barrier coatings by laser surface treatment. *Materials & Design*. 2014;57:336–341. <https://doi.org/10.1016/j.matdes.2013.12.075>
12. Nikhil A. P., Balasubramanian K. Biological and mechanical enhancement of zirconium dioxide for medical applications. *Ceramics International*. 2020;46(4):4041–4057. <https://doi.org/10.1016/j.ceramint.2019.10.220>
13. Chaoxi S., Jinshuang W., Xianjun L., Tingyang C., Mingyi X., Guang D., Yuancheng R., Zhongwei L., Zhixig D., Yifeng X., Guoqiang L., Yixing Z., Fuhe Y., Xueqiang C. Investigation of corrosion resistance of YSZ coating with sacrificial aluminum oxide protective layer against CMAS and composite corrosives. *Journal of the European Ceramic Society*. 2024;44(4):2537–2579. <https://doi.org/10.1016/j.jeurceramsoc.2023.11.030>
14. Clarke D.R., Phillpot S.R. Thermal barrier coating materials. *Materials Today*. 2005;8(6):22–29. [https://doi.org/10.1016/S1369-7021\(05\)70934-2](https://doi.org/10.1016/S1369-7021(05)70934-2)
15. Padture N.P., Gell M., Jordan E.H. Thermal barrier coatings for gas-turbine engine applications. *Science*. 2002;296(5566):280–284. <https://www.science.org/doi/10.1126/science.1068609>
16. Buinachev S., Mashkovtsev M.A., Zhirenkina N., Aleshin D., Dankova A. A new approach for the synthesis of monodisperse zirconia powders with controlled particle size. *International Journal of Hydrogen Energy*. 2021;46(32):16878–16887. <https://doi.org/10.1016/j.ijhydene.2021.01.134>
17. Yuzhuo L., Zhen Z., Xin W., Rende M., Limin H., Zhenhua X. Thermo-physical properties, morphology and thermal shock behavior of EB-PVD thermal barrier coat-

- ing with DLC YbGdZrO/YSZ system. *Materials Today Communications*. 2023;35:106265.  
<https://doi.org/10.1016/j.mtcomm.2023.106265>
18. He W., Mauer G., Sohn Y.J., Schwedt A., Guillon O., Vaßen R. Investigation on growth mechanisms of columnar structured YSZ coatings in plasma spray-physical vapor deposition (PS-PVD). *Journal of the European Ceramic Society*. 2019;39(10):3129–3138.  
<https://doi.org/10.1016/j.jeurceramsoc.2019.04.003>
  19. Gao L., Guo H., Wei L., Li C., Xu H. Microstructure, thermal conductivity and thermal cycling behavior of thermal barrier coatings prepared by plasma spray physical vapor deposition. *Surface and Coatings Technology*. 2015;276:424–430.  
<https://doi.org/10.1016/j.surfcoat.2015.06.033>
  20. Jude S.A.A., Winowlin Jappes J.T., Adamkhan M. Thermal barrier coatings for high-temperature application on superalloy substrates: A review. *Materials Today: Proceedings*. 2022;60(3):1670–1675.  
<https://doi.org/10.1016/j.matpr.2021.12.223>
  21. Vaßen R., Jarligo M.O., Steinke T., Mack D. E., Stöver D. Overview on advanced thermal barrier coatings. *Surface and Coatings Technology*. 2010;205(4):938–942.  
<https://doi.org/10.1016/j.surfcoat.2010.08.151>
  22. Shan Y., Gao L. Synthesis and characterization of phase controllable ZrO<sub>2</sub>-carbon nanotube nanocomposites. *Nanotechnology*. 2005;16(6):625–630.  
<https://doi.org/10.1088/0957-4484/16/6/001>
  23. Fenech J., Dalbin M., Barnabe A., Bonino J.P., Ansart F. Sol-gel processing and characterization of (RE-Y)-zirconia powders for thermal barrier coatings. *Powder Technology*. 2011;208(2):480–487.  
<https://doi.org/10.1016/j.powtec.2010.08.046>
  24. Chen C.Y., Tseng T.K., Tsai S.C., Lin C.K., Lin H.M. Effect of precursor characteristics on zirconia and ceria particle morphology in spray pyrolysis. *Ceramics International*. 2008;34(2):409–416.  
<https://doi.org/10.1016/j.ceramint.2006.10.013>
  25. Zhang H., Lu H., Zhu Y., Fan L., Duan R., Zhang M., Wang X. Preparations and characterizations of new mesoporous ZrO<sub>2</sub> and Y<sub>2</sub>O<sub>3</sub>-stabilized ZrO<sub>2</sub> spherical powders. *Powder Technology*. 2012;227:9–16.  
<https://doi.org/10.1016/j.powtec.2012.02.007>
  26. Buinachev S., Mashkovtsev M., Dankova A., Zhirenkina N., Kharisova K. Synthesis of YSZ powders with controlled properties by the CDJP method. *Powder Technology*. 2022;399:117201.  
<https://doi.org/10.1016/j.powtec.2022.117201>
  27. Carter G.A., Ogden M.I., Buckley C.E., Maitland C., Paskevicius M. Ammonia-induced precipitation of zirconyl chloride and zirconyl-yttrium chloride solutions under industrially relevant conditions. *Powder Technology*. 2009;188:222–228.  
<https://doi.org/10.1016/j.powtec.2008.04.087>
  28. Trovarelli A., Leitenburg C., Boaro M., Dolcet G. The utilization of ceria in industrial catalysis. *Catalysis Today*. 1999;50: 353–367.  
[https://doi.org/10.1016/S0920-5861\(98\)00515-X](https://doi.org/10.1016/S0920-5861(98)00515-X)
  29. Agarkova E.A., Borik M.A., Bublik V.T., Volkova T.V., Kulebyakin A.V., Kuritsyna I.E., Larina N.A., Lomonova E.E., Milovich F.O., Myzina V.A., Ryabochkina P.A., Tabachkova N.Yu. Effect of the phase composition and local crystal structure on the transport properties of the ZrO<sub>2</sub>-Y<sub>2</sub>O<sub>3</sub> and ZrO<sub>2</sub>-Gd<sub>2</sub>O<sub>3</sub> solid solutions. *Russian Microelectronics*. 2019;48:8:523–530.  
<https://doi.org/10.17073/1609-3577-2018-3-156-165>

## Information about the authors

**Sergei V. Buinachev** – Laboratory Assistant-researcher of the Department of Rare Metals and Nanomaterials, Ural Federal University named after the first President of Russia B.N. Yeltsin (UrFU); Junior Researcher of the Laboratory of Ceramics, Institute of High Temperature Electrochemistry of Ural Branch of the Russian Academy of Sciences (IHTE UB RAS).

<https://orcid.org/0000-0001-7722-9055>

E-mail: s.v.buinachev@urfu.ru

**Maksim A. Domashenkov** – Laboratory Assistant-researcher of the Department of Rare Metals and Nanomaterials, UrFU; Junior Researcher of the Laboratory of Ceramics, IHTE UB RAS.

<https://orcid.org/0009-0003-8882-9373>

E-mail: maks84155@gmail.com

## Информация об авторах

**Сергей Владимирович Буйначев** – лаборант-исследователь кафедры редких металлов и наноматериалов, Уральский федеральный университет имени первого Президента России Б.Н. Ельцина (УрФУ); мл. науч. сотрудник лаборатории керамики, Институт высокотемпературной электрохимии (ИВТЭ) УрО РАН.

<https://orcid.org/0000-0001-7722-9055>

E-mail: s.v.buinachev@urfu.ru

**Максим Александрович Домашенков** – лаборант-исследователь кафедры редких металлов и наноматериалов, УрФУ; мл. науч. сотрудник лаборатории керамики, ИВТЭ УрО РАН.

<https://orcid.org/0009-0003-8882-9373>

E-mail: maks84155@gmail.com

**Maksim A. Mashkovtsev** – Cand. Sci. (Chem.), Researcher of the Laboratory of Electrochemical Devices and Fuel Cells, IHTe UB RAS.

<https://orcid.org/0000-0002-4914-262X>

E-mail: maxftf@yandex.ru

**Dmitry O. Polivoda** – Junior Researcher of the Laboratory of Electrochemical Devices and Fuel Cells, IHTe UB RAS.

<https://orcid.org/0000-0002-3514-9919>

E-mail: sbbthblack@gmail.com

**Nina V. Zhirenkina** – Cand. Sci. (Eng.), Senior Researcher of the Laboratory of Advanced Functional Materials, UrFU.

<https://orcid.org/0000-0002-5823-9554>

E-mail: nina\_zhirenkina@mail.ru

**Максим Алексеевич Машковцев** – к.х.н., науч. сотрудник лаборатории электрохимических устройств и топливных элементов, ИВТЭ УрО РАН.

<https://orcid.org/0000-0002-4914-262X>

E-mail: maxftf@yandex.ru

**Дмитрий Олегович Поливода** – мл. науч. сотрудник лаборатории электрохимических устройств и топливных элементов, ИВТЭ УрО РАН.

<https://orcid.org/0000-0002-3514-9919>

E-mail: sbbthblack@gmail.com

**Нина Валерьевна Жиренкина** – к.т.н., ст. науч. сотрудник лаборатории перспективных функциональных материалов, УрФУ.

<https://orcid.org/0000-0002-5823-9554>

E-mail: nina\_zhirenkina@mail.ru

---

## Contribution of the authors

**S.V. Buinachev** – processed experimental data, wrote the manuscript, participated in the discussion of the results.

**M.A. Domashenkov** – conducted experiments, wrote the manuscript, processed documents for submitting the manuscript, participated in the discussion of the results.

**M.A. Mashkovtsev** – designed the experiment plan, revised the manuscript.

**D.O. Polivoda** – processed experimental data, graphical visualization of data.

**N.V. Zhirenkina** – graphical visualization of data, conducted experiments.

## Вклад авторов

**С.В. Буйначев** – обработка экспериментальных данных, написание текста статьи, участие в обсуждении результатов.

**М.А. Домашенков** – проведение экспериментов, написание текста статьи, участие в обсуждении результатов.

**М.А. Машковцев** – составление плана экспериментов, редактирование текста статьи.

**Д.О. Поливода** – обработка экспериментальных данных, графическая визуализация результатов исследований.

**Н.В. Жиренкина** – графическая визуализация данных, проведение экспериментов.

---

*The article was submitted 05.12.2023, revised 08.02.2024, accepted for publication 15.02.2024*

*Статья поступила в редакцию 05.12.2023, доработана 08.02.2024, подписана в печать 15.02.2024*